Fast 3D thick mask model for full-chip EUVL simulations

Peng Liu*, Xiaobo Xie, Wei Liu, Keith Gronlund
ASML Brion Technologies, 4211 Burton Drive, Santa Clara, CA, USA 95054

ABSTRACT

Extreme ultraviolet lithography (EUVL) uses a 13.5nm exposure wavelength, all-reflective projection optics, and a reflective mask under an oblique illumination with a chief ray angle of about 6 degrees to print device patterns. This imaging configuration leads to many challenges related to 3D mask topography. In order to accurately predict and correct these problems, it is important to use a 3D mask model in full-chip EUVL applications such as optical proximity correction (OPC) and verifications. In this work, a fast approximate 3D mask model developed previously for full-chip deep ultraviolet (DUV) applications is extended and greatly enhanced for EUV applications and its accuracy is evaluated against a rigorous 3D mask model.

Keywords: EUV, 3D mask, best focus shift, pattern shift, shadowing effect

1. INTRODUCTION

Extreme ultraviolet lithography (EUVL) is a promising technology for 1x node and below logic and memory device patterning. It uses a 13.5nm exposure wavelength, all-reflective projection optics, and a reflective mask under an oblique illumination with a chief ray angle of about 6 degrees. While these reflective imaging conditions are required because conventional optical materials are highly absorptive at the EUV wavelength, they also cause many undesired effects related to 3D mask topography. Even though EUVL uses a much shorter wavelength to image relatively large feature sizes (as compared to the wavelength) than deep ultraviolet (DUV) lithography, it actually has more 3D mask topography related challenges, which include pattern-dependent best focus shift, pattern shift, and shadowing effect.

Pattern-dependent best focus shift is not unique to EUV lithography. It has been observed in DUV lithography in many cases already[1-3]. The root cause can be traced to the 3D mask topography induced phase distortions in the transmitted field of a DUV mask[3]. Similarly, the 3D topography of an EUV mask can also introduce pattern-dependent phase distortions in the reflected field, resulting in best focus variations among different device features on the wafer and therefore degradation in the common process window. Other effects are more unique to EUV lithography as they originate from the reflective imaging configuration of the oblique chief ray angle in conjunction with the 3D mask topography. This configuration leads to a generally asymmetric illumination seen by the mask and, therefore, some EUVL-specific printing effects which are not seen or can be avoided in the imaging configuration of DUV lithography. One of such effects is asymmetric shadowing effect that presents itself as HV print bias between horizontal (H) and vertical (V) features. Although it can be modeled to a certain degree using the rule-based HV mask bias in the thin mask model[4], the accuracy becomes inadequate as the feature size reduces[5]. Pattern shift is another such effect caused by mask-side non-telecentricity due to the oblique chief ray angle. It is important to note that the large global pattern shift observed in early EUV simulations using 3D mask models is largely a modeling artifact and can be corrected by transforming the mask diffraction coefficient to the optimum object plane before passing it to the subsequent simulation steps[4-5]. This process mimics the EUV scanner setup stage that moves the mask to the optimum mask focal plane. However there still exists a residual, pattern-dependent pattern shift caused by the 3D mask topography even after the mask is placed at the optimum mask focal plane. Therefore 3D mask topography plays an important role in many of the challenges in EUV lithography. In order to accurately predict and correct these problems, it is important to use a 3D mask model in full-chip EUVL applications such as optical proximity correction (OPC) and verifications.

Although rigorous 3D mask models based on methods such as finite difference time domain (FDTD)[6] and rigorous coupled wave analysis (RCWA)[7] are available, they are computationally too expensive for large area or full-chip applications. In this work, a fast approximate 3D mask model developed previously for full-chip DUV applications is extended and greatly enhanced for EUV applications, and its accuracy is evaluated against a rigorous 3D mask model.

*peng.liu@asml.com, 1-408-200-0843

Extreme Ultraviolet (EUV) Lithography IV, edited by Patrick P. Naulleau, Proc. of SPIE Vol. 8679, 86790W
© 2013 SPIE · CCC code: 0277-786X/13/$18 · doi: 10.1117/12.2010818

Downloaded From: http://spiedigitallibrary.org/ on 05/06/2013 Terms of Use: http://spiedl.org/terms

In the following sections, we first discuss some special considerations in EUVL simulations with rigorous 3D mask models. These considerations are required in order to obtain realistic simulation results. Then we describe the development of the fast 3D mask model for full-chip EUV applications, followed by simulation case studies to validate its accuracy against a rigorous 3D mask model. A summary of this work is given in the end.

2. EUVL SIMULATION CONSIDERATIONS

Due to limited availability of experimental data for future device dimensions, the rigorous simulation remains the main vehicle to study the various effects in EUV lithography. In this work rigorous simulations will be used to generate reference data to evaluate the accuracy of the fast 3D mask model. Therefore it is important to carry out the rigorous simulations properly to ensure valid results are obtained.

2.1 Mask defocus effect

As EUV lithography uses a reflective mask illuminated with an oblique chief ray angle, the condition of telecentricity is no longer satisfied on the mask side as compared to DUV lithography. Consequently the effects of mask defocus are much more significant in EUV lithography. This aspect is particularly evident in lithography simulations using rigorous 3D mask models. In these simulations the transmitted (DUV) or reflected (EUV) mask fields are generally sampled at a pre-determined plane close to the top surface of the mask features. If these mask fields are directly used for subsequent image simulations, which implies that the sample plane is chosen as the object plane of the project lens, the images obtained at its conjugate image plane may not be optimum in terms of image contrast and pattern shift. As shown in Figure 1, the distance between the object plane and the sample plane is referred to as the mask defocus in this work.

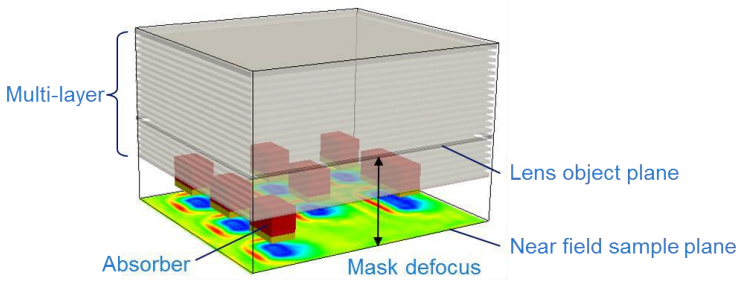


Figure 1: Definition of mask defocus for this work

From modeling point of view, the mask defocus effect may be ignored in DUV simulations, but it cannot be ignored in EUV simulations, especially for pattern shift. Note the effect of mask defocus is similar to wafer defocus but on a much smaller scale. It can be shown that the image change due to a mask defocus of Δ_m is approximately equivalent to a wafer defocus of $\Delta_w=M^2\Delta_m$ for low NA imaging, where M is the magnification of the projection lens. For a 4x reduction system, $M^2=1/16$. For CD control this effect may be ignored or largely compensated by a small change in wafer defocus. But for pattern shift, it is a quite different situation between DUV and EUV.

Many factors can contribute to the image shift of a pattern with respect to its position on the mask, including pattern symmetry, source symmetry, lens aberration, phase error induced by 3D mask topography, mask defocus, wafer defocus, etc... We will only consider an aberration-free system in this work. For a symmetric pattern, it can be easily shown that the pattern shift caused by the defocus and/or 3D mask topography can be cancelled out exactly by using a symmetric illumination pupil shape. This condition is generally satisfied in practical DUV applications. Therefore the mask defocus effect rarely needs to be modeled in DUV simulations. However, due to the reflective mask and the oblique chief ray angle employed by EUV lithography, it is impossible to make a symmetric illumination pupil shape from the mask viewpoint. As a result the pattern shift in EUV is not as trivial as in DUV. The contribution from the mask defocus is significant and generally global across all patterns. In addition, a mask pattern sees a slightly different illumination pupil

Downloaded From: http://spiedigitallibrary.org/ on 05/06/2013 Terms of Use: http://spiedl.org/terms

shape depending on its slit location. As a result, this global pattern shift on the field scale is shown as magnification error as a function of mask defocus.

In practice, the global pattern shift is minimized during the scanner setup stage where the mask is driven to the optimum mask focal plane. It is important to model the same process in EUV simulations that use rigorous 3D mask models. Otherwise the resulting wafer image may show a large global pattern shift, which in reality is just a modeling artifact of not choosing the object plane properly. An example is shown in Figure 2, which compares the resist contours simulated by directly using the sample plane as the object plane to those simulated after moving the object plane to 180nm behind the sample plane. The mask simulations in this example were done using an ASML Brion in-house rigorous electromagnetic field (EMF) solver for Maxwell's equations based on the FDTD method. A large global pattern shift of several nanometers is observed in simulation when the object plane is placed at the sample plane. But it can be corrected in simulation by moving the object plane to the optimum location, which mimics the scanner setup process.

Note, for all the simulations presented in this work, an EUV system of numerical aperture NA=0.33, magnification M=0.25 and chief ray angle at object (CRAO) = 6° is used. The resist CDs and contours are computed from optical images using a constant threshold. No actual resist models are used or required as the 3D mask effects are optical effects.

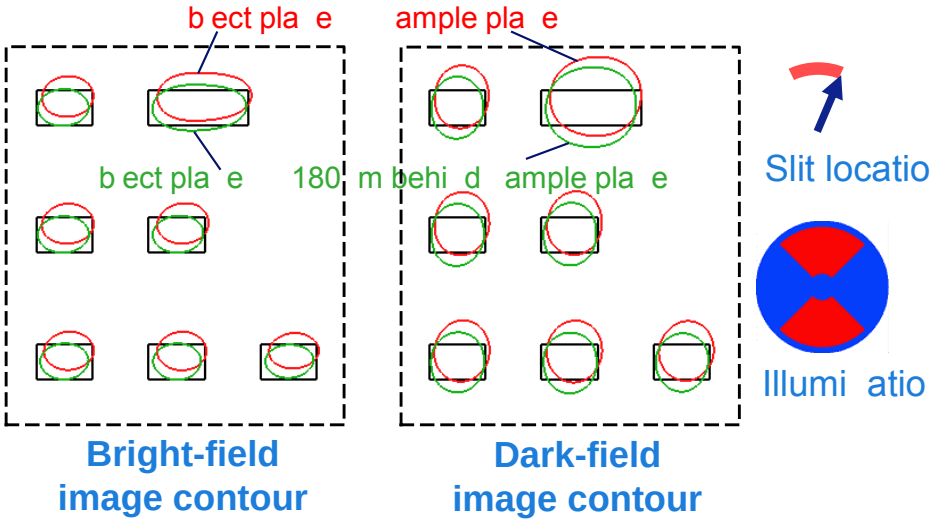


Figure 2: Comparison of the resist contours simulated by directly using the sample plane as the object plane (red contours) to those simulated after moving the object plane 180nm behind the sample plane (green contours)

2.2 Incident angle effect

In a lithography application the mask is generally illuminated by a partially coherent source. From modeling point of view, the source can be considered as a collection of planewaves, each is incoherent from others and illuminates the mask at a given incident angle. In low-NA DUV lithography simulations, the incident angle effect can be modeled using the so-called Hopkins approach, which assumes that the two transmitted fields produced by two plane waves of different angle of incidence differ by only a shift in spectral space. The diffraction order amplitude and relative phase remain the same. It is now well known that the Hopkins approach can introduce significant errors in high-NA DUV lithography simulations[8]. For the state-of-the-art DUV scanner of 1.35NA, the maximum angle of incidence on the mask is close to 20 degrees. Rigorous mask simulations show that the relative phase in diffraction orders changes significantly over this range of angle of incidence. If not properly taken into account, it can produce wrong results in best focus shift predictions, which have been confirmed by both experiments and rigorous simulations[3].

The current most advanced EUV system under evaluation has NA of 0.33 and chief ray angle of 6 degrees. Figure 3 shows the range of incident angle distribution on the EUV mask as compared to the DUV mask. Note the big circle in Figure 3 represents the maximum incident angle (~20 degrees) on the DUV mask. The center represents the normal incidence on the mask. The three smaller circles represent the range of the incident angle distribution on the EUV mask for the slit center and two opposite edge locations, respectively. Since the incident angle distribution is much narrower on the EUV mask, it is reasonable to assume that the mask near field simulated at the chief ray angle may be

Downloaded From: http://spiedigitallibrary.org/ on 05/06/2013 Terms of Use: http://spiedl.org/terms

representative enough for the entire source. This turns out to be an acceptable assumption from CD and best focus prediction point of view. But it may not be adequate for pattern shift prediction depending on the accuracy requirement.

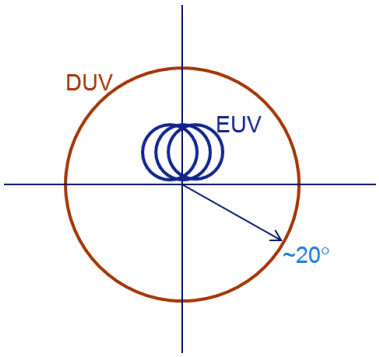


Figure 3: Comparison of the range of incident angle distribution on mask between EUV and DUV

A straightforward method to model the incident angle effect of a partially coherent illumination is to decompose the illumination pupil shape into smaller sections[9]. The angle of incidence is considered constant within each section and therefore only one rigorous 3D mask simulation is required to compute its contribution to the wafer image using Hopkins approach. The total wafer image is the sum of the images produced by individual sections. The result is expected to converge as the number of sections increases.

A simulation work was carried out to study the convergence as a function of the number of incident angles used for rigorous EUV mask simulations. The illumination pupil shape and the incident angle locations are shown in Figure 4(a). The pupil shape is the same as that shown in Figure 2 and is used to illuminate the mask at the slit edge.



Figure 4(a): Pupil shape and incident angle locations used for rigorous 3D mask simulations

We investigated both bright-field and dark-field masks having horizontal (H) and vertical (V) lines or spaces of width=12nm and pitch=100nm on wafer scale. The simulation was done using HyperLith's RCWA-based rigorous 3D mask model. We pre-scanned the mask defocus and selected a value to minimize the global patterns shift. This value was then fixed for all the simulations. Figure 4(b) shows the results of Bossung curves of XCD (CD of V line/space) and YCD (CD of H line/space). It is apparent that the number of angles has very small effect on CD and best focus shift. One angle of incidence at the chief ray may be considered adequate. It is also worth noting that the best focus shift is pattern-dependent between horizontal and vertical features, caused by 3D mask topographies.

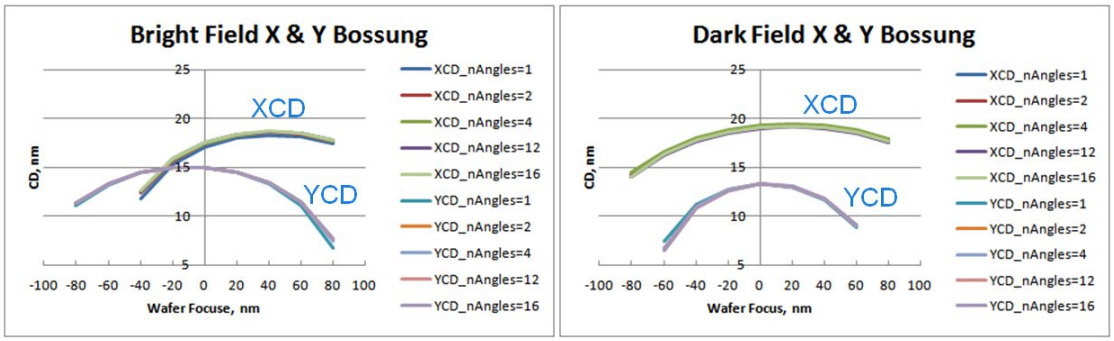


Figure 4(b): Convergence of Bossung curve as a function of the number of incident angles used for rigorous 3D mask simulations. XCD = CD of V line/space. YCD = CD of H line/space.

Downloaded From: http://spiedigitallibrary.org/ on 05/06/2013 Terms of Use: http://spiedl.org/terms

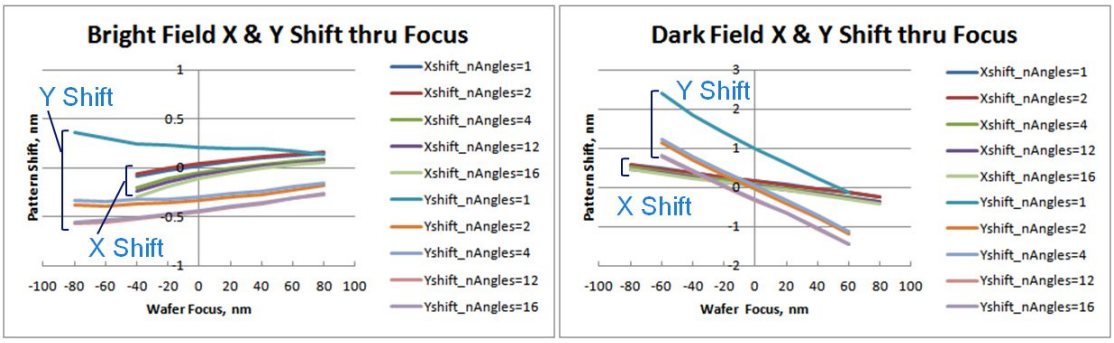


Figure 4(c): Convergence of thru-focus pattern shift as a function of the number of incident angles used for rigorous 3D mask simulations. X Shift = pattern shift of V line/space. Y Shift = pattern shift of H line/space

The convergence is however quite different for pattern shift. As shown in Figure 4(c), using only the chief ray angle can cause over 1nm error in pattern shift prediction and incorrect thru-focus trend. At least two incident angles, one for each pole, are required to reduce the error to below 0.5nm and to obtain the correct trend. More are needed to further reduce the error. But it is not going to be very practical for 2D pattern simulations as they are very time consuming. In this example, up to 12 incident angles may be required to obtain a near converged result.

3. FAST 3D MASK MODEL DEVELOPMENT

In this section we describe the extension and enhancement of a fast approximate 3D mask model for full-chip EUV applications. This model was developed previously for full-chip DUV applications and showed good accuracy in best focus shift predictions as compared to rigorous models and experiments[3]. The details of its development are given in the previous work[10] and therefore not repeated here. In the following discussions, we first summarize the key elements of the previous model as they are the foundation of the present work. Then we describe the additional development made in this work to extend it for full-chip EUV applications.

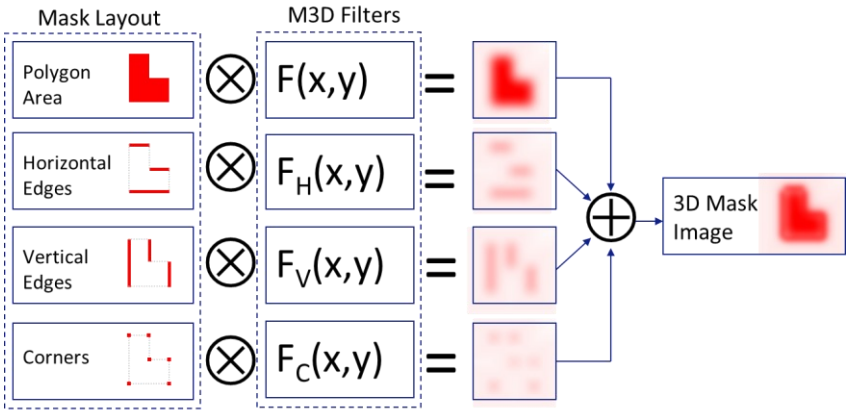


Figure 5: Illustration of the working principle of the fast 3D mask model

As discussed in our previous work, the fast 3D mask model developed for DUV lithography consists of the following key elements. First of all, the mask image of a given pattern is computed by convolving the layout properties such as polygon area and edges with the so-called M3D filters. This process is illustrated in Figure 5. For a coherent illumination

Downloaded From: http://spiedigitallibrary.org/ on 05/06/2013 Terms of Use: http://spiedl.org/terms

this mask image is directly related to the transmitted field of the mask. For a partially coherent illumination it does not have a direct association with a measureable physical property. It is more of an intermediate mathematical property that is to be convolved with the Transmission Cross Coefficient (TCC) of Hopkins theory to obtain the wafer image. Therefore the model accuracy is determined by the mask image and in turn by the M3D filters. We construct these filters from a library of transmitted fields of representative mask features, pre-computed using a rigorous EMF solver for Maxwell's equations. The use of a rigorous EMF solver ensures that the relative phase between diffraction orders can be captured besides amplitude. Note this phase information is completely missing in the thin mask model but plays an important role in determining the best focus of a given pattern. In addition, the relative phase greatly depends on the incident angle. In order to capture this dependency, an array of transmitted fields of various incident angles needs to be included in the rigorous library simulations. Then, for a given partially coherent illumination, we combine these rigorous library fields according to its pupil shape to compute the filters. The oblique incidence effect is thus embedded in these filters. One set of filters can be computed for the entire pupil or a sub-section of the pupil depending on the accuracy requirement. In a full-chip simulation these filters are re-used to compute the mask images for each patch of mask patterns.

It has been shown that the above model is capable of accurately predicting the best focus shift observed in rigorous simulations and experiments in DUV applications. In this work, it is further extended and enhanced for EUV applications. It is referred to as M3D+ model in this work as opposed to the previous M3D model. The basic working principle of this model stays the same as shown in Figure 5. The new developments are mainly in the area of M3D+ filter generation that takes into account mask defocus effect and edge-to-edge interaction effect. These new developments are illustrated in Figure 6, followed by more detailed discussions on each of the components.

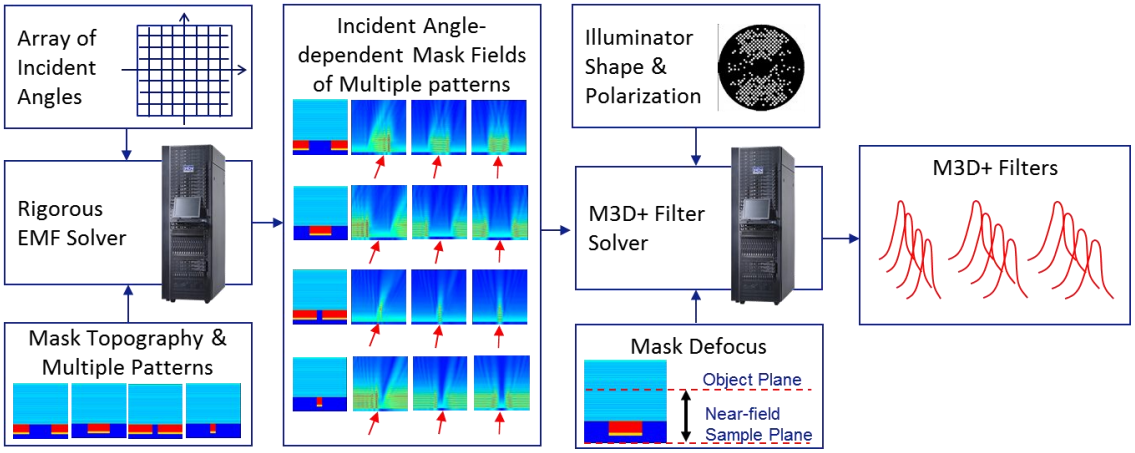


Figure 6: Illustration of M3D+ filter generation for EUVL simulations

3.1 Library generation for EUV mask

EUV lithography uses a reflective mask as opposed to a transmissive mask in DUV lithography. Therefore, instead of transmitted fields, the reflected fields of representative EUV mask features need to be rigorously simulated and stored in the library. The reflected fields at various incident angles, not just the chief ray angle, are also required in order to capture the incident angle effect of a partially coherent source in EUV lithography.

3.2 Mask defocus

As discussed in the previous section, the mask defocus has a significant effect on the results of EUV simulations with 3D mask models. It is important to model the scanner setup process that moves the mask to the optimum mask focal plane. To enable this capability, the previous fast 3D mask model is extended to include the mask defocus function. It is implemented by first propagating the library fields from the sample plane to the object plane as specified by the mask defocus and then constructing the filters from the new library fields. Note that, since the mask defocus effect is included in the filters, there is no runtime impact in OPC and verification applications. The optimum mask defocus can be determined by mimicking the scanner setup process that minimizes the global pattern shift.

Downloaded From: http://spiedigitallibrary.org/ on 05/06/2013 Terms of Use: http://spiedl.org/terms

3.3 Edge-to-edge interaction

From modeling point of view, the total EMF scattering effect of a mask may be separated into two parts – the primary scattering effect and the secondary scattering effect. The former refers to the EMF scattering effect of individual feature edges, including the interference effect of these individually scattered fields. The latter refers to the interaction effect that a scattered field being scattered again by nearby edges and so on. The secondary scattering effect is usually much smaller than the primary scattering effect. It may be ignored in many cases where the edge separation is large and/or the feature height is small so that the interaction is weak.

As the device feature sizes continue to shrink, the modeling errors introduced by edge-to-edge interactions begin to show appreciable impact to the CD and overlay error budget. This effect is particularly apparent for EUV lithography because the absorber height is much larger than the wavelength and comparable to the spaces of dense features, making it more susceptible to interactions with the scattered fields from neighboring edges. The edge-to-edge interaction effect in EUV mask may be conceptually illustrated in Figure 7(a), where the largest arrow represents the incident field and the smaller solid arrows represent the primary scattered field from the left edge. Part of this scattered field hits the nearby right edge and is scattered again, resulting in a secondary scattered field.

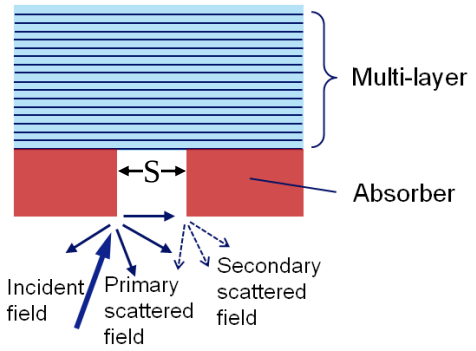


Figure 7(a): Conceptual illustration of edge-to-edge interaction in EUV mask

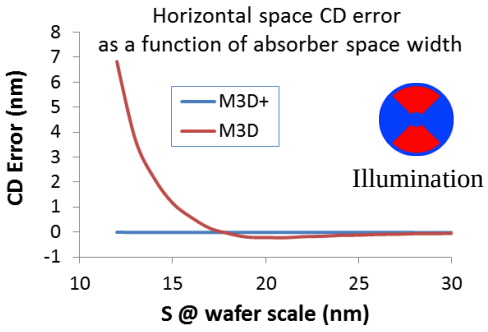


Figure 7(b): Model accuracy comparison between M3D (w/o edge-to-edge interaction effect taken into account) and M3D+ (w/ interaction effect taken into account)

In this work we have extended the previous model by adding rigorous simulations of edge interaction fields as part of the library generation. These additional library fields enable us to extract the edge-to-edge interaction effect and build additional filters. By applying these filters we are able to include the edge-to-edge interaction effect in full-chip EUVL simulations.

A simulation example is shown in Figure 7(b) which compares the model accuracy as a function of absorber space between the M3D model (w/o the edge-to-edge interaction effect taken into account) and the M3D+ model (with the interaction effect taken into account). The CD error refers to the difference between the CD predicted by the M3D/M3D+ model and that by the rigorous FDTD model. As the space becomes smaller than 17nm (wafer scale), the M3D CD error starts to increase significantly while M3D+ maintains an excellent accuracy. The pitch is fixed at 100nm in this example. More accuracy evaluations on the M3D+ model are discussed in the next section.

Note the above method for edge-to-edge interaction modeling is not limited to EUVL, it can be used for DUV simulations as well.

4. MODEL ACCURACY VALIDATION

In this section we evaluate the accuracy of the fast 3D mask model against rigorous results for EUVL simulations. Two case studies were carried out, one on 1D patterns and the other on 2D patterns. The in-house FDTD EMF solver was used to generate the reference data for these studies as it is more memory efficient than RCWA for 2D pattern simulations. The benchmark between these two rigorous EMF solvers showed good agreement for the 1D test case presented in Section 2. The comparison is shown below in Figure 8.

Downloaded From: http://spiedigitallibrary.org/ on 05/06/2013 Terms of Use: http://spiedl.org/terms

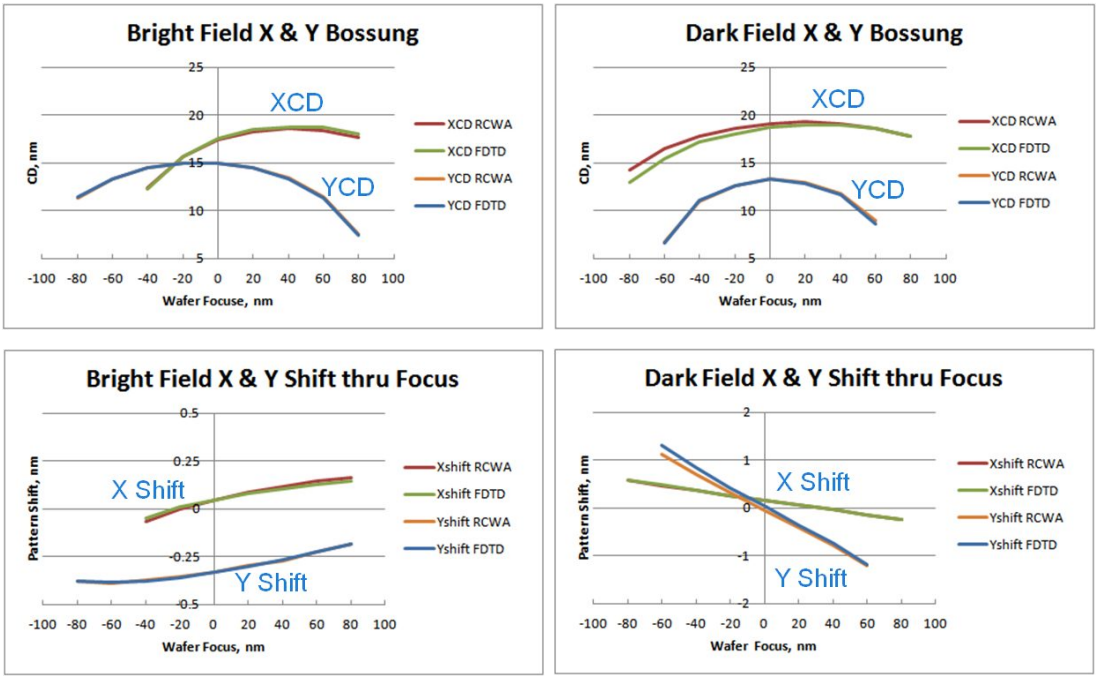


Figure 8: Comparison of simulation results between RCWA and FDTD

In the following discussions we present the comparison between the fast 3D mask model M3D+ and the rigorous 3D mask model FDTD. The comparison to thin mask model is also included as appropriate.

4.1 1D pattern case study

The 1D patterns used in this study consist of H/V lines (for bright-field mask) or spaces (for dark-field mask) of width from 10nm to 30nm, pitch from 28nm to 40nm with 2nm increment and from 40nm to 100nm with 10nm increment. Rigorous simulations were done first to generate the reference CD data for a range of focus-exposure matrix (FEM) conditions. The H and V line/space CD's of the largest feature (i.e., 30nm lines or spaces with 100nm pitch) at the center slit location under the nominal FEM condition were used to calibrate the threshold of the M3D+ model. A thin mask model was also calibrated, which included HV mask bias in addition to threshold. The calibrated model was then used to predict CDs and pattern shift of all features at both center and edge slit locations under the full range of FEM conditions. The results were compared with the rigorous reference data.

Figure 9 shows the M3D+ and thin mask model RMS of predicted CD delta to rigorous FDTD model. The RMS was calculated across all features per slit location, FEM condition and mask type. The prediction power is significantly improved by the M3D+model over the thin mask model.

The issue with the thin mask model is the lack of the prediction capability for pattern-dependent best focus shift and HV bias. An example is given in Figure 10, which compares the Bossung curves between the thin mask model and FDTD for 12nm and 30nm lines/spaces having 100nm pitch under the nominal dose condition. Clearly, the thin mask fails to capture the pattern-dependent best focus shift. In addition, the HV mask bias that works for large features fails to work for small features, particularly for the dark-field mask.

The M3D+ is not shown in Figure 10 because it is on top of FDTD almost exactly in this example. More detailed Bossung comparisons between M3D+ and FDTD are given in Figures 11(a-d).

The comparison of pattern shift between M3D+ and FDTD is shown in Figures 12(a-c). Thin mask model is not shown as it cannot capture this effect.

Downloaded From: http://spiedigitallibrary.org/ on 05/06/2013 Terms of Use: http://spiedl.org/terms

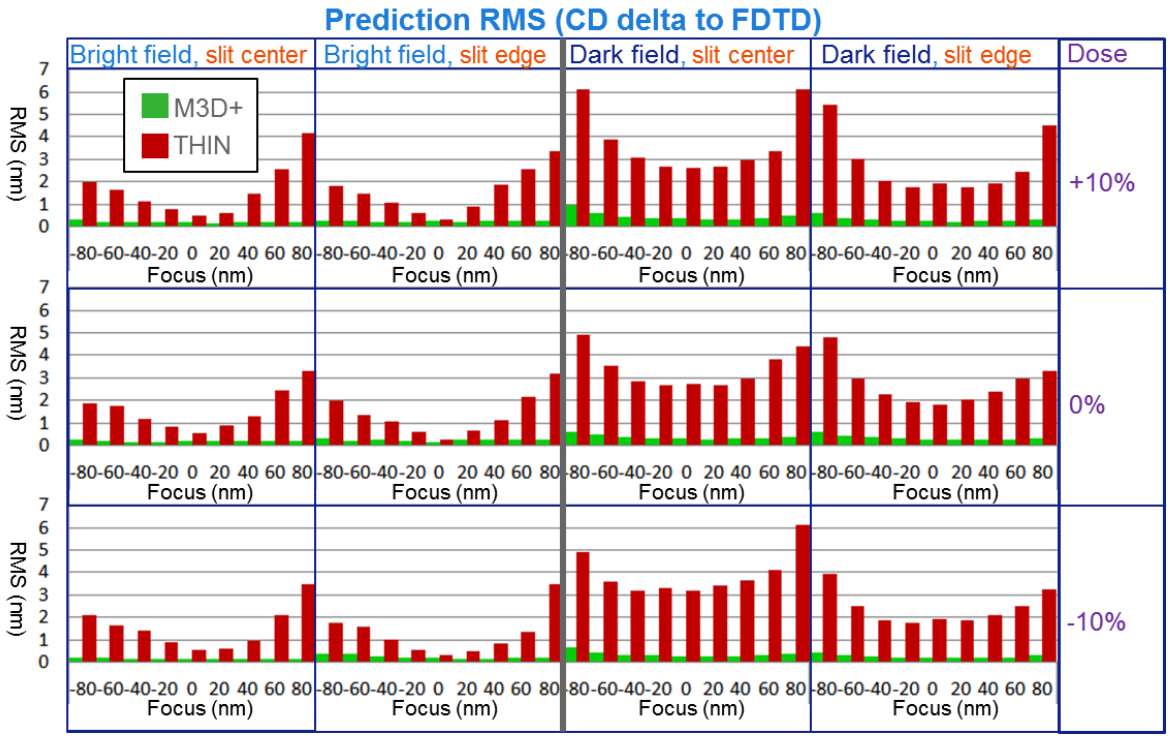


Figure 9: M3D+ and thin mask model RMS of predicted CD delta to FDTD. The RMS was calculated across all features per slit location, FEM condition and mask type. The issue with the thin mask model is the lack of the prediction capability for pattern-dependent best focus shift and HV bias (see Figure 10).

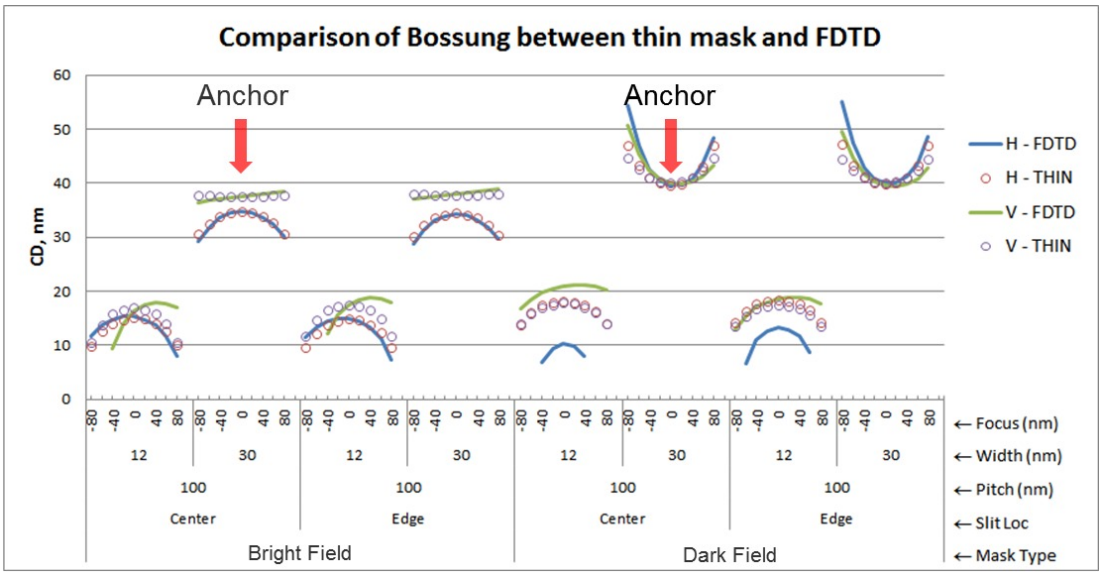


Figure 10: Comparison of Bossung curves between thin mask model and FDTD under the nominal dose condition. The thin mask fails to capture the pattern-dependent best focus shift. In addition, the HV bias that works for large features in the thin mask model fails to work for small features, particularly for the dark-field mask.

Downloaded From: http://spiedigitallibrary.org/ on 05/06/2013 Terms of Use: http://spiedl.org/terms

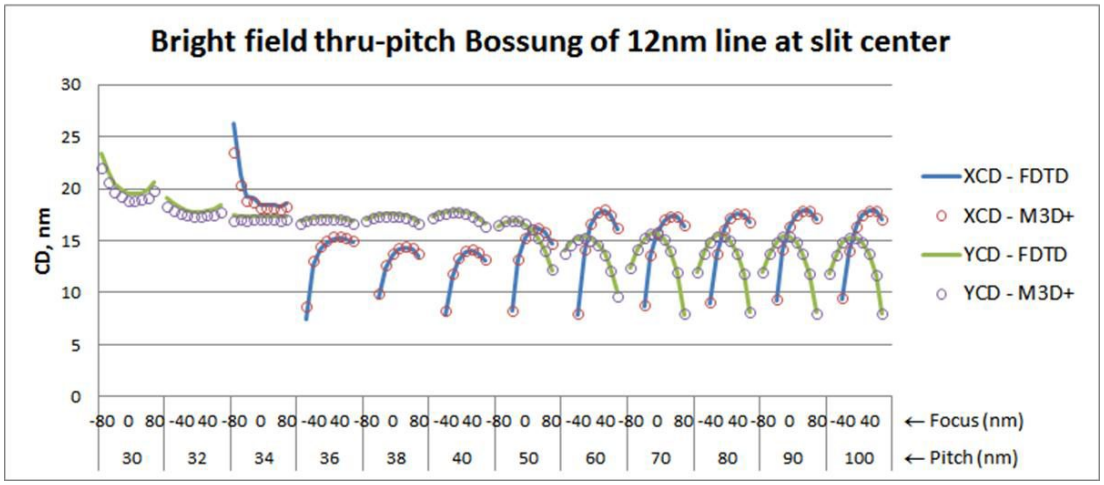


Figure 11(a): Bright field thru-pitch Bossung of 12nm line at slit center under the nominal dose condition

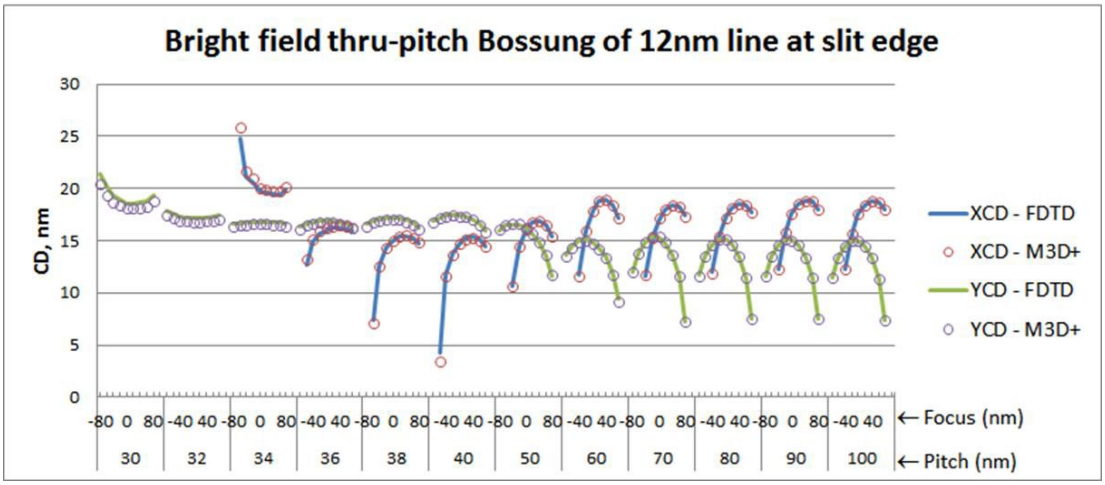


Figure 11(b): Bright field thru-pitch Bossung of 12nm line at slit edge under the nominal dose condition

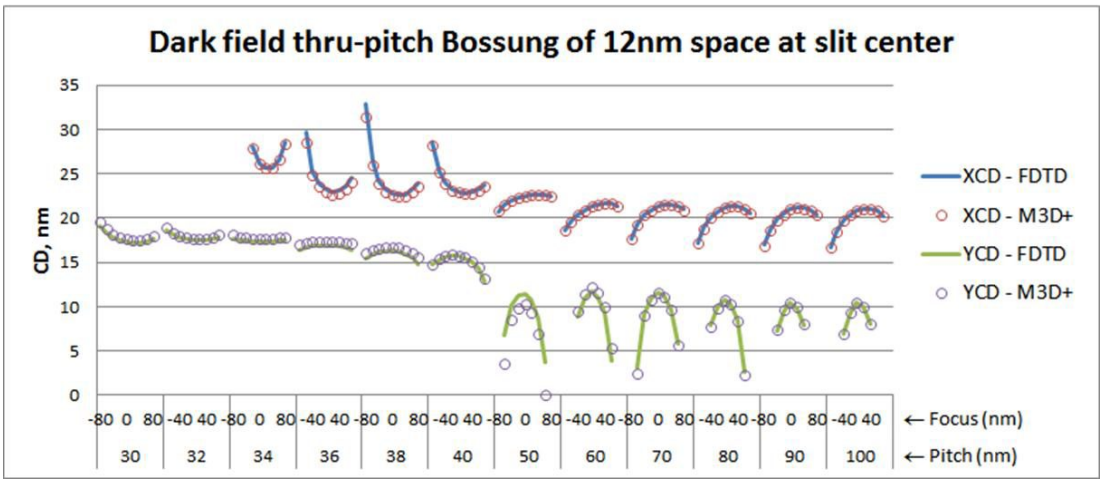


Figure 11(c): Dark field thru-pitch Bossung of 12nm space at slit center under the nominal dose condition

Downloaded From: http://spiedigitallibrary.org/ on 05/06/2013 Terms of Use: http://spiedl.org/terms

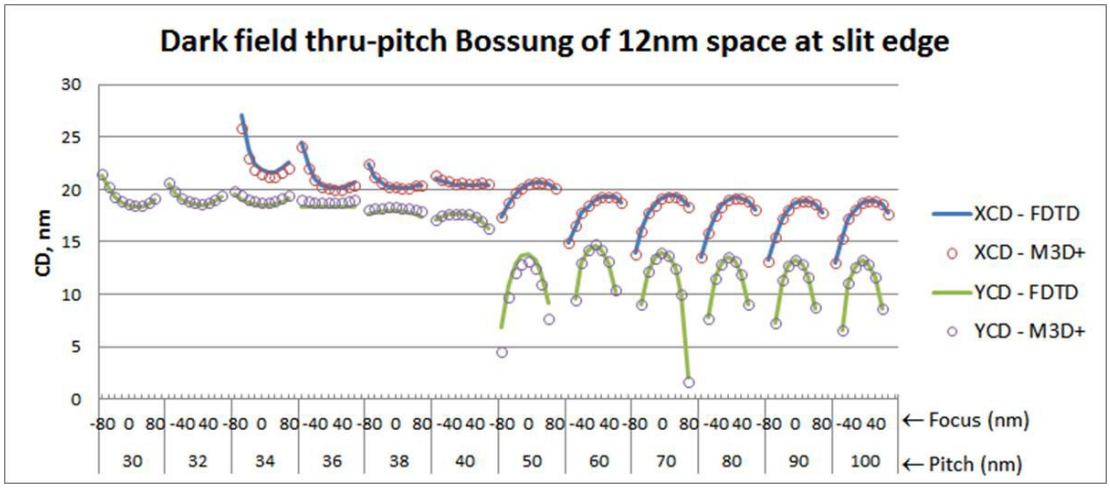


Figure 11(d): Dark field thru-pitch Bossung of 12nm space at slit edge under the nominal dose condition

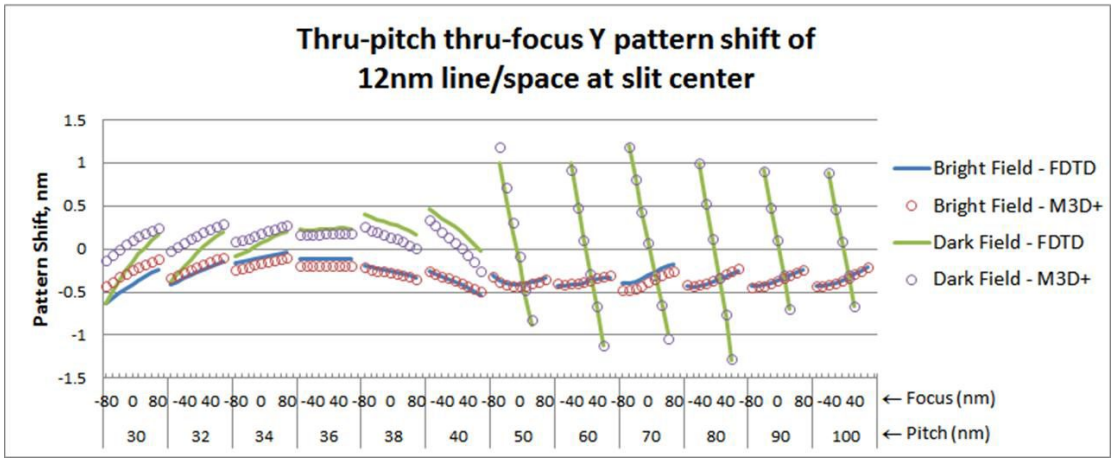


Figure 12(a): Thru-pitch thru-focus Y shift of 12nm line (dark field) and space (bright field) at slit center under the nominal dose condition

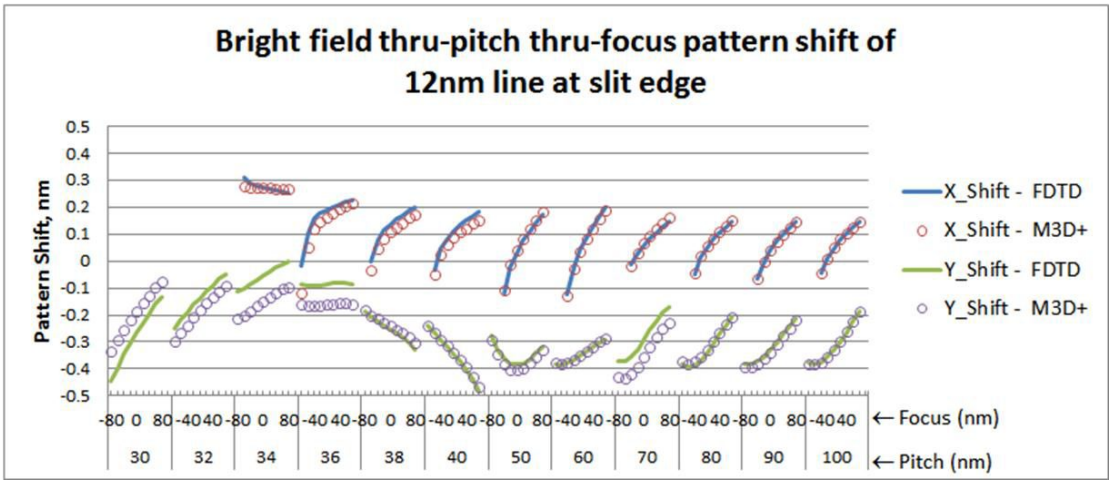


Figure 12(b): Bright field thru-pitch thru-focus pattern shift of 12nm line at slit edge under the nominal dose condition

Downloaded From: http://spiedigitallibrary.org/ on 05/06/2013 Terms of Use: http://spiedl.org/terms

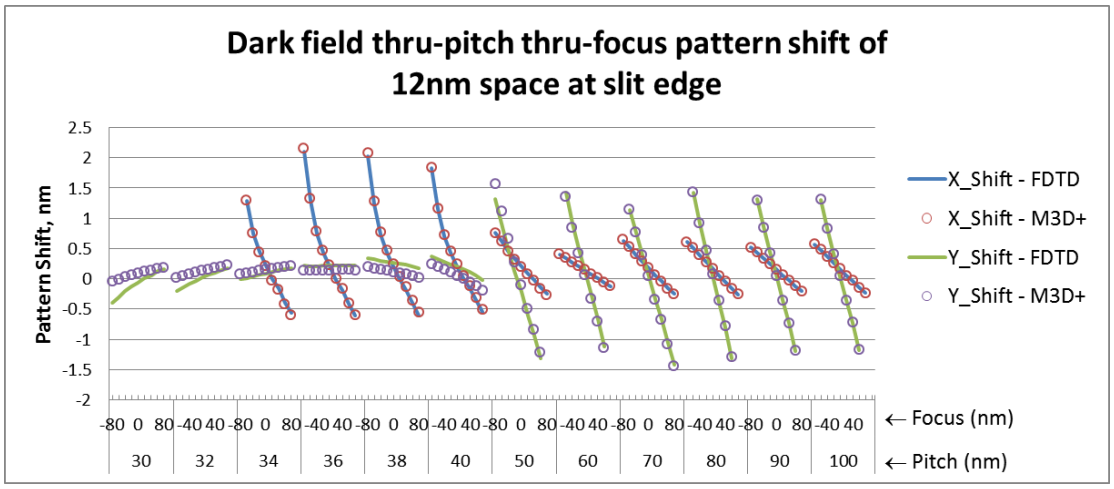


Figure 12(c): Dark field thru-pitch thru-focus pattern shift of 12nm space at slit edge under the nominal dose condition

4.2 2D pattern case study

2D patterns of an actual design are much more diverse compared to 1D patterns. To make this study more relevant, we adopted the 2D patterns previously investigated by a device manufacturer, which highlighted the need of 3D mask modeling in EUV applications[11]. These patterns are shown in Figure 13.

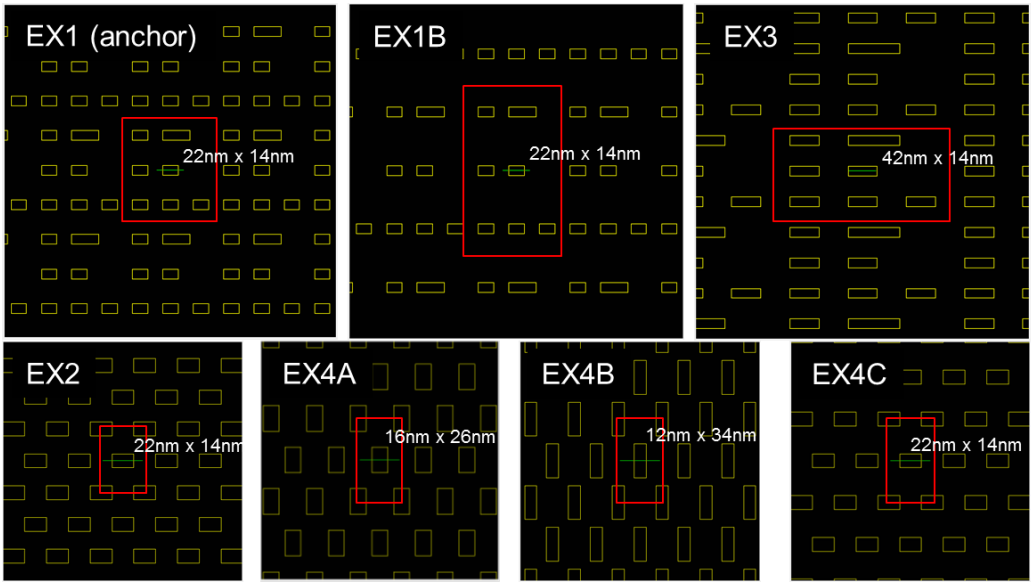


Figure 13: 2D patterns used in simulation

The size of the feature at the simulation domain center is labeled. In this work these patterns were directly used in simulations without any OPC. Again, rigorous simulations were done first to generate reference data. The X- and Y-CD's of the first pattern (EX1) at the slit center under the nominal FEM condition were used to calibrate the M3D+ model and the thin mask model. Only threshold was calibrated for the M3D+ model. For the thin mask model, HV bias was also calibrated in addition to threshold. Then the calibrated model was used to predict the printed contours of all patterns and compared to rigorous results. The RMS of predicted CD delta to FDTD is shown in Figure 14.

Downloaded From: http://spiedigitallibrary.org/ on 05/06/2013 Terms of Use: http://spiedl.org/terms

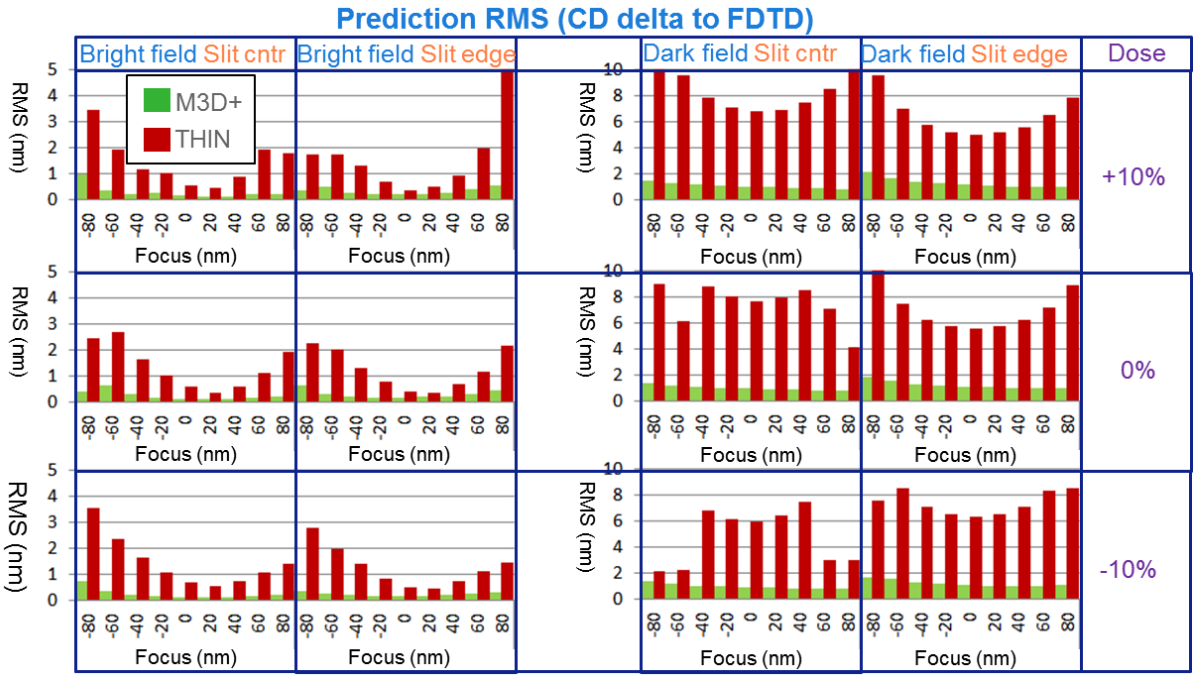


Figure 14: M3D+ and thin mask model RMS of predicted CD delta to FDTD. The RMS was calculated across all features per slit location, FEM condition and mask type. One pattern was removed from the thin mask dark-field RMS calculation as it was not printed under the thin mask model (some thin mask model data points under off-nominal conditions were also removed for the same reason).

Note one pattern was removed from the thin mask dark-field RMS calculation as it was not printed under the thin mask model (some thin mask model data points under off-nominal conditions were also removed for the same reason). But it was printed in the FDTD model. As shown in Figure 15 which compares the Bossung between thin mask and FDTD, the thin mask model CD of EX4B is reported as zero since the pattern fails to print. The dark-field mask generally has lower image quality, especially when without OPC, and therefore a small error in image can result in a large error in contour defined by threshold. For the same reason, the M3D+ model RMS is worse on the dark-field mask than the bright-field mask, although it is significantly improved over the thin mask model. More detailed comparisons between M3D+ and FDTD are given in Figure 16 on Bossung curves and in Figure 17 on pattern shift.

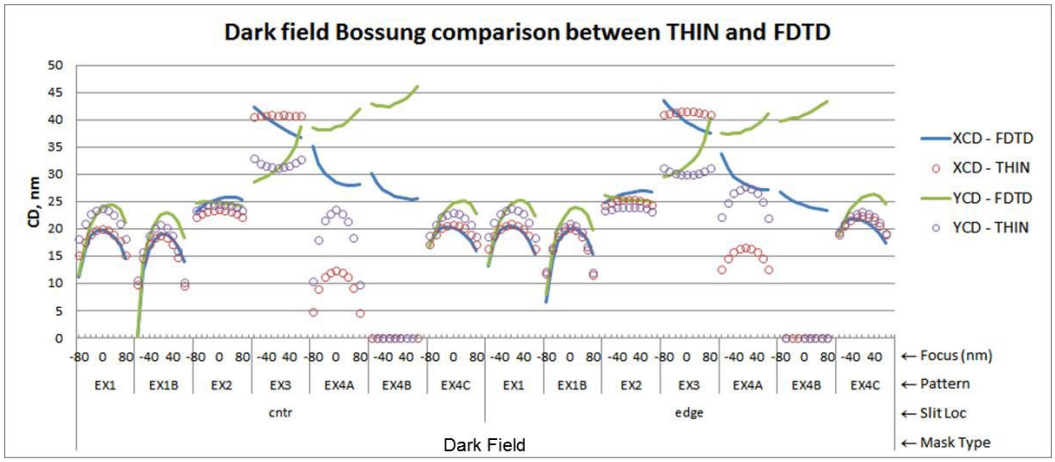


Figure 15: Dark field Bossung comparison between thin mask and FDTD under the nominal dose condition. Note the thin mask model CD of EX4B is reported as zero since the pattern fails to print. It was removed from the thin mask model RMS calculation.

Downloaded From: http://spiedigitallibrary.org/ on 05/06/2013 Terms of Use: http://spiedl.org/terms

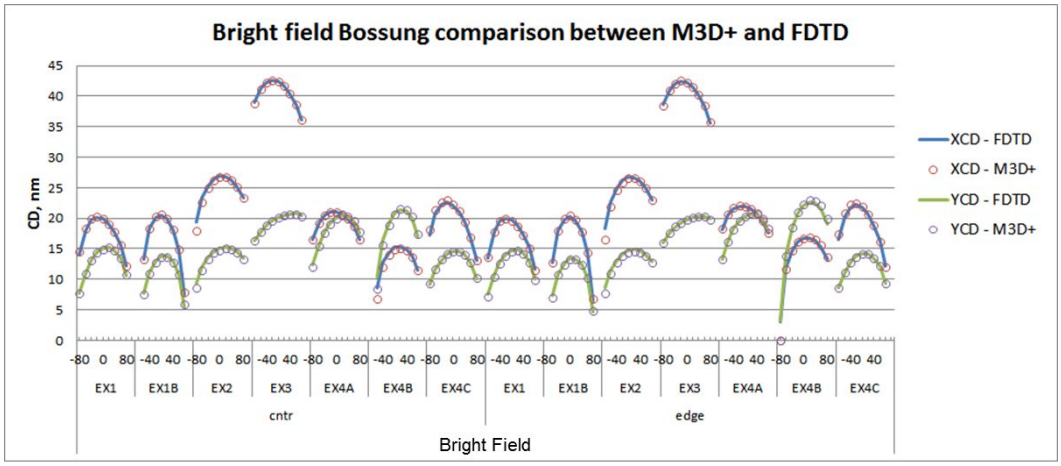


Figure 16(a): Bright field Bossung comparison between M3D+ and FDTD under the nominal dose condition

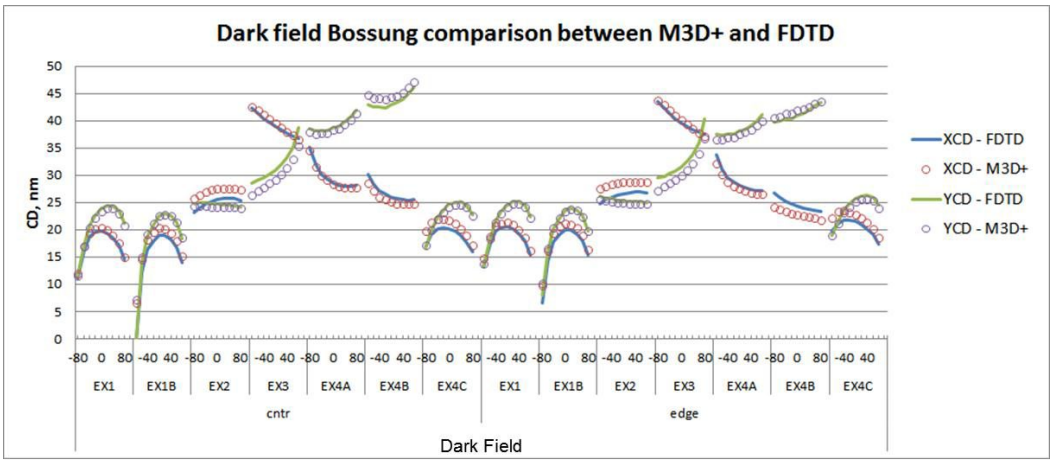


Figure 16(b): Dark field Bossung comparison between M3D+ and FDTD under the nominal dose condition

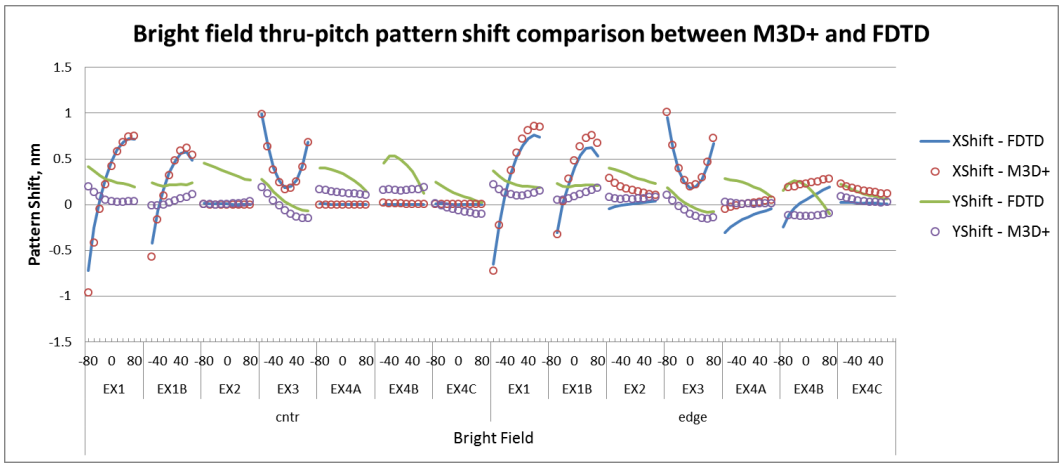


Figure 17(a): Bright field pattern shift comparison between M3D+ and FDTD under the nominal dose condition

Downloaded From: http://spiedigitallibrary.org/ on 05/06/2013 Terms of Use: http://spiedl.org/terms

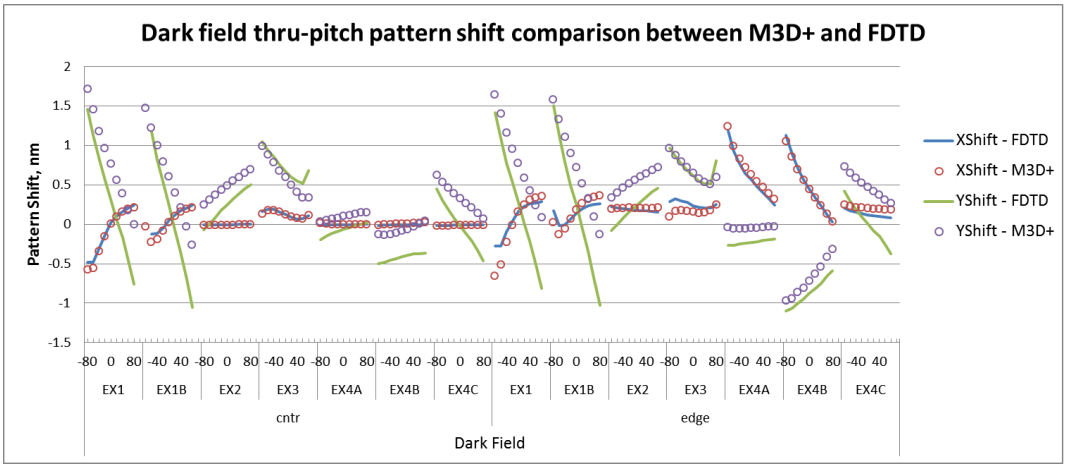


Figure 17(b): Dark field pattern shift comparison between M3D+ and FDTD under the nominal dose condition

5. SUMMARY

We have discussed the special considerations on mask defocus and incident angle effects in rigorous EUVL simulations using 3D mask models. The optimum mask defocus needs to be determined first by mimicking the scanner setup process so that the global pattern shift or magnification error is minimized. Unlike in DUV simulations, the incident angle has only a small effect on CD and best focus prediction in EUV simulations. But it has a significant impact to pattern shift prediction.

In this work we have extended and enhanced a fast 3D mask model developed previously for full-chip DUV applications to EUV applications. The new development includes modeling of mask defocus and edge-to-edge interaction effects. Case studies were carried out to evaluate its accuracy against a rigorous 3D mask model for 1D and 2D patterns in both bright-field and dark-field masks. The fast 3D mask model showed significant accuracy improvement over the thin mask model. It accurately captured the Bossung shift/tilt as predicted by the rigorous model. It also captured the pattern shift within about 0.5nm error. It is worth pointing out that pattern shift simulations in general require more accurate models. More improvement in this area may be needed depending on the overlay control requirement.

ACKNOWLEDGMENT

The authors would like to thank Ming Ding, Song Lan, Jun Chen and Mu Feng for their assistance in development and evaluation of the model.

REFERENCES

[1] Frank Staals et al., “Advanced Wavefront Engineering for Improved Imaging and Overlay Applications on a 1.35 NA Immersion Scanner,” Proc. of SPIE Vol. 7973, 2011

[2] Jo Finders and Thijs Hollink, “Mask 3D effects: impact on Imaging and Placement,” 27th European Mask and Lithography Conference, Proc. of SPIE Vol. 7985, 2011

[3] Peng Liu, “Accurate prediction of 3D mask topography induced best focus variation in full-chip photolithography applications,” Proc. of SPIE Vol. 8166, 816640 (2011)

[4] Hoyoung Kang, Steve Hansen, Jan van Schoot and Koen van Ingen Schenau, "EUV simulation extension study for mask shadowing effect and its correction", Proc. SPIE 6921, Emerging Lithographic Technologies XII, 69213I (March 21, 2008)

Downloaded From: http://spiedigitallibrary.org/ on 05/06/2013 Terms of Use: http://spiedl.org/terms

[5] Gregory McIntyre, Chiew-seng Koay, Martin Burkhardt, Hiro Mizuno and Obert Wood, "Modeling and experiments of non-telecentric thick mask effects for EUV lithography", Proc. SPIE 7271, Alternative Lithographic Technologies, 72711C (March 17, 2009)
[6] Allen Taflove, Susan C. Hagness, "Computational Electrodynamics: The Finite-Difference Time-Domain Method," Artech House; 3 edition (June 30, 2005)
[7] M. G. Moharam and T. K. Gaylord, "Rigorous coupled-wave analysis of planar-grating diffraction," JOSA, Vol. 71, Issue 7, pp. 811-818 (1981)
[8] Andreas Erdmann, Peter Evanschitzky, and Peter De Bisschop, "Mask and Wafer Topography Effects in Immersion Lithography," Optical Microlithography XVIII, edited by Bruce W. Smith, Proceedings of SPIE Vol. 5754 (SPIE, Bellingham, WA, 2005)
[9] Andreas Erdmann, Giuseppe Citarella, Peter Evanschitzky, Hans Schermer, Vicky Philipsen, and Peter De Bisschop, "Validity of the Hopkins approximation in simulations of hyper NA (NA>1) line-space structures for an attenuated PSM mask," Optical Microlithography XIX, edited by Donis G. Flagello, Proc. of SPIE Vol. 6154, 61540G, (2006)
[10] Peng Liu et al, "Fast and accurate 3D mask model for full-chip OPC and verification," Proc. of SPIE Vol. 6520, 65200R, (2007)
[11] Yan Borodovsky (Intel), "EUV Lithography at Insertion and Beyond," 2012 International Workshop on EUV Lithography, Maui, Hi

Downloaded From: http://spiedigitallibrary.org/ on 05/06/2013 Terms of Use: http://spiedl.org/terms